Structure and electrical properties of the spin 1/2 one-dimensional antiferromagnet Ca_2CuO_3 prepared by the sol–gel technique

2007 J. Phys.: Condens. Matter 19 106215

(http://iopscience.iop.org/0953-8984/19/10/106215)

IOP PUBLISHING JOURNAL OF PHYSICS: CONDENSED MATTER

J. Phys.: Condens. Matter **19** (2007) 106215 (8pp) doi:10.1088/0953-8984/19/10/106215

Structure and electrical properties of the spin 1/2 one-dimensional antiferromagnet Ca_2CuO_3 prepared by the sol–gel technique

Dang-Chinh Huynh[1], **Duc-The Ngo**[2] **and Nam-Nhat Hoang**[3,4]

[1] Faculty of Chemical Technology, Hanoi University of Technology, 1 Dai Co Viet, Hanoi, Vietnam
[2] Department of Physics and Astronomy, University of Glasgow, Glasgow G12 8QQ, UK
[3] Centre for Materials Science, College of Science, Vietnam National University Hanoi, 334 Nguyen Trai Road, Hanoi, Vietnam

E-mail: nhathn@vnu.edu.vn

Received 11 January 2007
Published 23 February 2007
Online at stacks.iop.org/JPhysCM/19/106215

Abstract

Highly homogeneous finely powdered Ca_2CuO_3 has been prepared by the sol–gel technique. No evidence for CaO and CuO impure phases was observed. The single-phase purity was observably better than that of samples prepared by the ceramic method and oxalate co-precipitation. On the basis of the structural parameters determined, the bond valence sum approach was involved in explaining the weak interchain direct Cu–Cu covalent bonding. The I–V and $\rho(T)$ measurements showed constant semiconductor behaviour with resistivity increase above 10^8 Ω cm in the low temperature region. The fitting of $\rho(T)$ using a band gap model gave an activation energy as small as 0.19 eV. This finding demonstrates well the covalent insulator nature of this system.

1. Introduction

Since the discovery of high T_c superconducting ceramics, the strongly anisotropic, $S = 1/2$ quasi-1D antiferromagnet Ca_2CuO_3 containing infinite anionic CuO_3 chains has attracted continuous attention due to interesting physical issues and structural similarity to sister superconductors. The observed extremely low ordered moment and reduced Néel temperature (≈0.06 μ_B and 5 K for Sr_2CuO_3; 0.05(3) μ_B and 9 K for Ca_2CuO_3 [1, 2]) together with a record value among 1D systems for the intrachain exchange integral $J_\parallel \approx 0.2$ eV (1300 K) (whereas the interchain coupling is only $J_\perp \approx 0.01$ meV) [3, 4] have led several scientists to consider such compounds as 'superstars' in the field of low dimensional magnetism [5]. To date, Ca_2CuO_3 (and its derivatives) has been synthesized mainly via the ceramic route but the

[4] Author to whom any correspondence should be addressed.

achievement of single-phase Ca_2CuO_3 was known to be very difficult. According to present equilibrium phase diagrams for the CaO–CuO pseudo-binary system, the coexistence of phases Ca_2CuO_3, $CaCu_2O_3$, CaO and CuO, plus a liquid phase above 1020 °C, can be considered. Dou *et al* [6] has reported the preparation of Ca_2CuO_3 by the oxalate co-precipitation technique and showed that the Ca_2CuO_3 phase was formed at 800 °C and its proportion increased with the calcining temperature. But even after calcining at 870 °C for 48 h, a proportion of CuO phase was still present in the sample as observed in x-ray diffraction patterns (figure 1 in [6]). It was pointed out that the lattice parameters tend to increase with increasing CuO dissolution. Later, Wada *et al* [7] reported the structure of single-crystal Ca_2CuO_3 prepared by the travelling solvent floating zone (TSFZ) method using an excess CuO content of about 10 mol%. This deviation from the known phase diagrams, leading to impure phases, e.g. $CaCu_2O_3$ (<5%), was explained by the possible dissociation of CuO into Cu_2O and O_2 at high temperature which results in a deficit of reacting CuO, so requiring the adding of this component. The lattice parameters from the above two cases agree quite well with the recent report of Zhang *et al* [8], where $a = 3.257(3)$, $b = 3.776(9)$ and $c = 12.23(6)$ Å (ceramic route). These authors showed that under pressure up to 34 GPa, the lattice parameters reduced ≈5% in length and the resistance dropped from above 10^4 to nearly $10^{2.7}$ Ω. Unfortunately, inadequate information on preparation was given. So to get a single-phase powder of good quality for further preparation of new materials and study of electronic properties, we have prepared the Ca_2CuO_3 by the sol–gel route.

2. Experimental details

A mixture of $Ca(NO_3)_2$ and $Cu(NO_3)_2$ in the required molar proportion was dissolved in water and an aqueous solution of citric acid (CA) was added, keeping the CA/metal ion ratio within 1.6–2.0 according to the pH of the solution. Then with vigorous stirring, the ammonia solution was added slowly to maintain the pH within 3–3.5. A homogeneous transparent blue gel appeared after sequential heating up to 80 °C for a while. The blue gel was dried in air for a day to form a xerogel and calcined at 550 °C for several hours to burn off the organic compounds. The middle product was sintered at 920 °C for 24 h in open air to produce the final Ca_2CuO_3 powder which was then pressed into cylinders of 10 mm diameter and 1 mm height. Before calcination (at 550 °C), the xerogel was examined by DTA/TGA analysis (using a TA SDT 2960 system). For SEM and EDX analysis the Jeol 5410 LV and the Oxford ISIS 300 systems were used. For $\rho(T)$ measurement (figure 5), the Au contact was sputtered on both faces of the samples (by Leybold DC/RF Univex 450). For I–V measurement, only one face was sputtered while the other was attached to an ohmic contact. Besides, a reference sample was made by the ceramic route using the procedure described in [10] (the sintering temperature was 870 °C) from the source powder $CaCO_3$ (99.9%; Merck) and CuO (99.99%; MaTeck). The characteristics of this sample are also included in section 3 for comparison.

3. Results and discussion

Figure 1 shows the DTA and TGA analysis of the xerogel. One exothermal peak appeared at 470 °C and one endothermal peak at 800 °C. The peak at 470 °C with relatively large weight loss corresponds to the oxidation of organic substances where the peak at 800 °C corresponds to the forming of Ca_2CuO_3 phase which frees the excess O_2. This temperature agrees exactly with the one reported by Dou *et al* [6] for forming of Ca_2CuO_3 phase by the oxalate co-precipitation technique. Figure 2 shows the x-ray diffraction patterns of the samples made by ceramic and

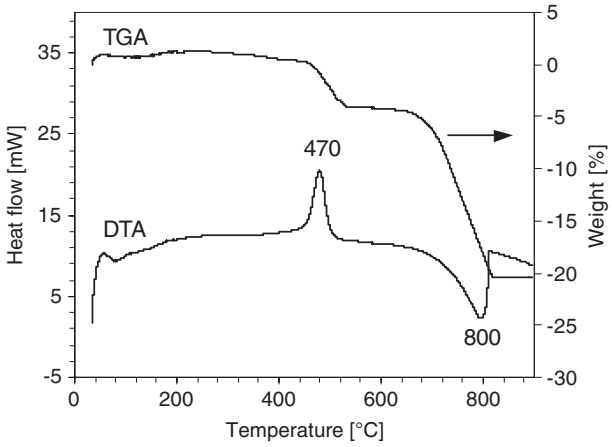

Figure 1. DTA and TGA analysis of the xerogel.

sol–gel routes. The indexing of peaks followed the $(-cba)$ axis orientation (used in [8]) rather than the (abc) orientation (used in [10] and in JCPDS Files [20]). In the $(-cba)$ orientation, the c axis is the longest axis. These diffractograms were taken on the Bruker D5005 system and analysed by the Rietveld technique using WinMProf software [21]. The ceramic sample showed traces for both CaO and CuO phases as indicated by peaks (200), (220) (CaO) and (110), (111), (200) (CuO). Except (110) (CuO), all these peaks—especially the (200) (CaO)—also appeared in the diffractogram given by Zhang *et al* [8] (ceramic route). In comparison to this, our sample seemed to have the same quality and showed a similar tendency towards having been enriched by a small proportion of CaO phase. For the ceramic route, the amount of CuO present in the final product was comparable to the amount of CaO whereas for the oxalate co-precipitation technique [6], there was no evidence for CaO but the intensity of the peak pair (111, 200) (CuO)—indicating the presence of a larger amount of CuO—was significantly stronger. The sol–gel sample showed, on the other hand, only peaks for the Ca_2CuO_3 phase, but with two new ones: (011) and (004). These peaks are weak and were not observed before [6, 8]. It is important to note that they belong strictly to the Ca_2CuO_3 phase, not to the impurity. It was observed that they would be stronger if the Ca were to be substituted by elements with larger atomic x-ray scattering factors, e.g. by lead or uranium. Doing that, there would appear three more weak peaks in the diffractogram of Ca_2CuO_3: (112), (211) and (204) (shown by the down arrows in figure 2) [19]. The higher purity of phase for the sol–gel sample can easily be checked against the CaO and CuO peaks indicated by vertical bars placed immediately below the main diffractograms in figure 2. Figure 3(a) shows the EDX analysis for the sol–gel sample; no elements other than Ca, Cu and O were observed. The Raman scattering measurement (discussed elsewhere) also showed peaks for Ca_2CuO_3 phase only, not for either $CaCu_2O_3$ (ladder compound, $Pmmn$) or CuO ($C2/c$). The Fourier fitting for the peak shape using WinFit software [22] showed the average monocrystal size to be 32 nm which is about 20 times smaller than the average 640 nm for the polycrystalline particle size shown via SEM (figure 3(c)). For the ceramic sample, the monocrystal size was nearly the same but the particle size was significantly larger; it lies between 1 and 3 μm (figure 3(b)). The fact that the sol–gel derived diffractogram (figure 2) does not show peak broadening was probably caused by technological setting: the higher sintering temperature and longer sintering time were customized for the sol–gel route.

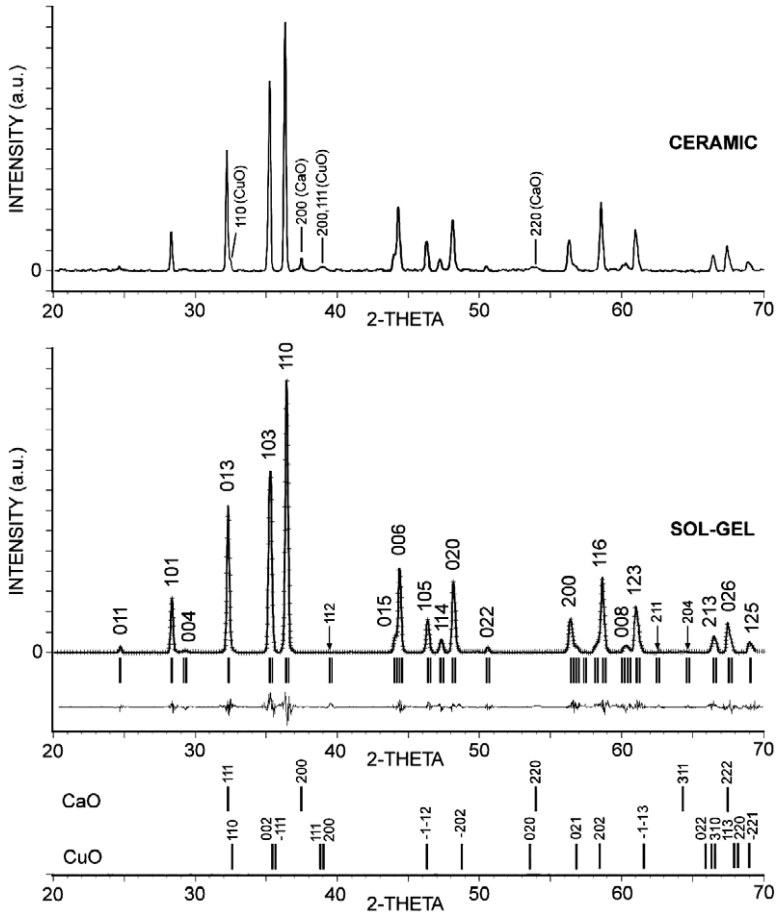

Figure 2. X-ray diffraction patterns for Ca_2CuO_3. The *hkl* indices of the Ca_2CuO_3 phase correspond to the $(-cba)$ axis orientation. For the ceramic sample, only peaks that do not correspond to Ca_2CuO_3 phase are indexed. For the sol–gel sample, the down arrows show minor peaks. The vertical bars at the bottom show the main peak positions for CaO and CuO phases with *hkl* indices given above each bar.

Figure 4 shows the structure of the Ca_2CuO_3 phase as refined in the $Immm$ space group (no. 71, D_{2h}^{25} in Schönflies notation). The profile refinement was carried out using the pseudo-Voigt function and included the scale factors, zero point, background, half-widths, correction to asymmetry and cell parameters in the first stage. After that the atomic coordinates and temperature factors were refined. Because of symmetry, only z coordinates of O(1) and Ca were allowed to vary; all other were fixed. The site occupation factors were also fixed except for those of the two oxygens. The Ca_2CuO_3 lattice differs from that of the La_2CuO_4 (2D system) only by one missing oxygen in the a direction. The CuO_4 plaquettes, sharing a corner oxygen O(2), are connected into infinite chains in the b direction with the Cu–O–Cu angle equal to 180°. Such a 1D arrangement is lacking in both a and c directions. The CuO_4 unit is not square, as the Cu–O bond is elongated in the c direction (1.96 Å versus 1.89 Å in the b direction). The interchain separation is 3.25 Å, exactly equal to the a axis one.

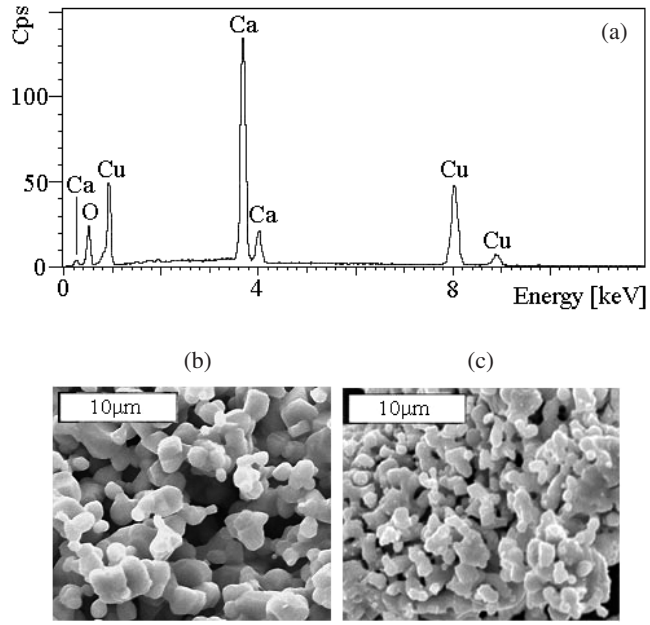

Figure 3. EDX spectrum for Ca_2CuO_3 sample (a); the SEM photograph of the surface for a reference sample made by the ceramic route (b) and for the sol–gel sample (c).

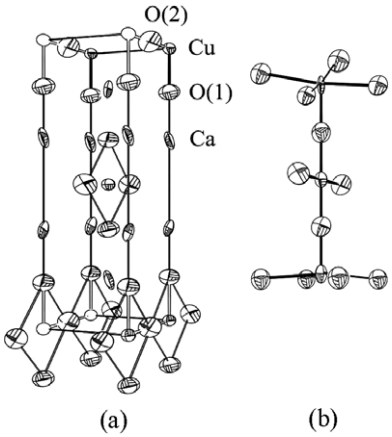

Figure 4. The structure of Ca_2CuO_3 from Rietveld analysis of powder data with thermal ellipsoids drawn by ORTEP [23] (a) and the bonding of atoms within the unit cell (b).

Table 1 gives bond lengths, isotropic thermal motion coefficients (B_{ISO}), estimated stoichiometry x (site occupation factors). It is worth noting from figure 4 that the anisotropic thermal motions of Ca atoms show excessive movement along the c axis. This was probably caused by the existence of only one Ca–O bond along this direction in the coordination pyramid O(1)–$CaO(1)_4$ which eased the Ca movement vertically. Thus the preferred vibration mode is the stretching axial motion, giving rise to the strong Raman allowed A_g mode phonons observed at 306 cm^{-1} [9]. The anisotropic thermal motion coefficients obtained from Rietveld refinement agree well with this observation.

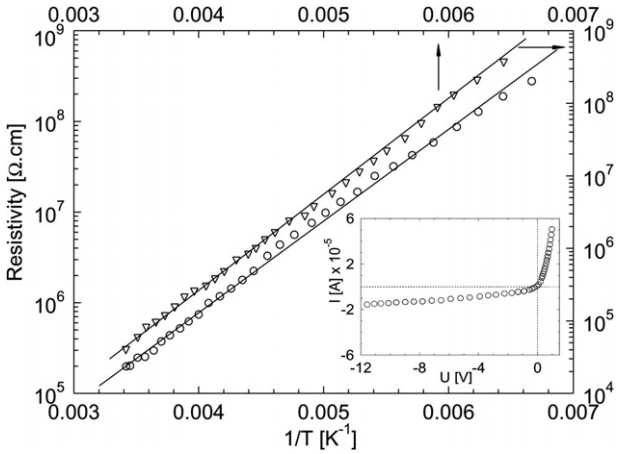

Figure 5. The thermal dependences of the resistivity for Ca_2CuO_3. Circles denote the sol–gel sample whereas triangles denote the ceramic one. The straight lines were fitted according to the band gap model. The p–n junction's I–V characteristic for the sol–gel sample at 300 K is featured in the inset.

Table 1. The structural parameters for Ca_2CuO_3. The standard deviations are given in parentheses. (Least square R-factors: R_F (intensity) = 4.2, R_P (profile) = 9.3, R_{WP} (weighted profile) = 10.4, S.G. = $Immm$, $a = 3.254(2)$, $b = 3.778(5)$, $c = 12.235(1)$ Å, $V = 150.4(5)$ Å^3.)

Atom	B_{ISO} (Å^2)	x	Bond	Length (Å)
Ca	0.23(2)	2	Cu–O(1)	1.958(4)
Cu	0.16(1)	1	Cu–O(2)	1.889(1)
O(1)	0.49(5)	0.98(2)	Cu $\cdots$ Cu	3.254(2)
O(2)	0.51(8)	1.0(3)	Cu–O(2)–Cu	3.778(5)

The high purity of the phase of the sol–gel sample allowed us to adopt the bond valence sum model for analysis of the relationship between the structure and electronic properties of Ca_2CuO_3. Basically there are two models for bond valences: the one derived from a Born–Landé type of potential [12] and the one based on minimization of the molecular orbital stabilization energy [16]. According to the first, the actual distributed valence within a given bond (e.g. to O) is estimated as $\exp[(R_0 - R)/B]$, where R is the bond length, R_0 and B are empirical constants. Using the bond lengths from table 1, the actual oxygen bonded valence of Cu is $+2.07$, and that of O is -2.01. These values show excellent agreement with the nominal oxidation state $+2/-2$ of Cu/O and with $+2.09$ for Cu reported in [10]. The second model uses the polynomial estimate $\sum a_i/R^i$ for bond valences and provided nearly the same result. So the structural parameters given in table 1 are believed to be correct.

This enables us to provide forecast of the direct interchain interaction between two Cu atoms. The possibility of Cu ions creating strong covalent bonding to the neighbouring Cu ions without changing the oxidation state is an interesting aspect of Cu bonding in cuprates. Such a direct Cu–Cu bond was observed experimentally for Cu_2O using convergent beam electron diffraction and x-ray charge density mapping by Zuo *et al* [13]. In Cu_2O the Cu has a full d shell $3d^{10}$ and an unoccupied $4s^1$ state. It has been shown that there was a hybridization of the Cu^{1+} $3d^2_{z^2}$ orbital with the higher unoccupied Cu^{1+} 4s orbital, which removed $0.22e$ from $3d^2_{z^2}$ and created an observable d hole. The distributed charge in the tetrahedral interstitial region of

four neighbouring Cu atoms was $\approx 0.2e$ Å^{-3}, suggesting a strongly covalent character of the Cu–Cu bonding. In Ca_2CuO_3 the Cu^{2+} ion has the electronic state $3d^9$ with a half-filled $d^1_{x^2-y^2}$ band and an empty 4s band. So theoretically there is enough room for relocation of charge from $3d^2_{z^2}$ orbital to the outer 4s. From the structural point of view, this process if it happens must be weaker than in Cu_2O because of the longer Cu–Cu distance (3.02 Å for Cu_2O instead of 3.25 Å for Ca_2CuO_3). To be precise, the 0.25 Å longer bond length induces a 50% lower bond valence, i.e. the shared valence in Cu^{2+}–Cu^{2+} is only $0.11e$, half of the $0.22e$ of Cu_2O. The weaker interchain covalent bonding in Ca_2CuO_3 has some support from theoretical calculation of the magnetic coupling ratio $J_\parallel/J_\perp$ of the intrachain and interchain couplings (parallel and perpendicular to axis b) on the basis of the t–J model which showed $J_\parallel/J_\perp = 321$ and the hopping parameter ratio $t_\parallel/t_\perp = 16$ [5, 14].

Figure 5 shows the thermal dependences of the resistivity measured with a sensitive four-electrode set-up for both sol–gel and ceramic samples. The I–V curve shown in the inset corresponds to the sample prepared by the sol–gel route and was measured for the p–n junction composed of a sample and different contacts (Schottky/Ohmic) at its two faces. The exponential shape of the I–V curves demonstrates the typical semiconductor behaviour of the sample. From this figure a thermally activated conduction mode can be expected. As the exponential characteristics remained unchanged on lowering the temperature, the conduction mode appeared to hold constant. The same was observed for the ceramic sample. Commonly there are three main approaches for interpreting the $\rho(T)$ curves obtained: the classical band gap model (T^{-1} law), the small polaron model (T^{-1} law) and the variable range hopping model ($T^{-1/4}$ law). For the Ca_2CuO_3, the usual way is to consider the hopping of small polarons since the observation of localized holes at oxygen sites associated with structural deformation provides a good supporting argument for it. However, as the fit did not give a satisfactory result at low temperature, we have tried the classical band gap law. The fitting according to this model gave thermal activation energy quite close to those values already reported, although the fit still showed a small deviation at lower temperature. Recently, the regime of percolative conduction through the grain boundary as the fractal conduction medium seemed to be essential for several Ru doped manganate and ruthenate perovskite ceramics [15] but due to the insulator character of Ca_2CuO_3 we do not expect it here.

To interpret $\rho(T)$ within the framework of the band gap model, the measured data were fitted with the expression $\ln\rho \propto E/k_BT$ and the thermal activation energy was determined from the slope. We obtained $E = 0.19$ eV for the sol–gel sample and 0.26 eV for the ceramic one. Both values are far below the 1.70 eV obtained via optical measurement [11] and seem to correspond to 0.18 eV reported on the basis of transport measurements [17, 18]. The occurrence of high resistivity in contrast to the relatively small thermal activation energy nicely illustrates the covalent insulation state in our samples. Unlike in pd metals where the upper Hubbard band falls within the O 2p orbital due to small intrachain hopping parameter t ($=\langle\psi_p|H|\psi_d\rangle$), in covalent insulators such as Ca_2CuO_3 the t increases according to the shortening of the intrachain Cu–O(2) length. Thus the energy separation between the Cu 3d–O 2p bonding state and the anti-bonding state enlarges. At certain finite t the compound becomes an insulator since the conduction band has lifted above the half-filled anti-bonding level serving as the insulating ground state [17]. Although the gap is small, the localization of holes at the oxygen sites is essential for the state of so-called covalent insulation.

A small increase in activation energy seen for the ceramic sample may be due to the presence of impurities which induces larger local distortion to Cu–O chain but may also come from the impure phases themselves. Commonly, the conduction mechanism in this system, and in ceramics too, is a complex problem, so further studies are needed to shed light on it.

4. Conclusions

Single-phase, high quality fine powder of the quasi-1D antiferromagnet Ca_2CuO_3 has been successfully synthesized by the sol–gel technique. It was demonstrated by careful structural analysis that this method has led to a better result than others such as the oxalate co-precipitation and ceramic routes. The 1D behaviour of Ca_2CuO_3 was clearly demonstrated by analysis of the Cu–Cu direct interaction along the *a* axis and the Cu–O–Cu coupling along the *b* axis. The measurement of the resistivity using a very sensitive four-electrode set-up has shown the continuous semiconductor behaviour with resistivity increased quickly to above 10^8 Ω cm in the low temperature region. The band gap model identified an activation energy as small as 0.19 eV, so with this value our sample manifests itself clearly as a typical covalent insulator.

References

[1] Yamada K, Wada J, Hosoya S, Endoh Y, Noguchi S, Kawamata S and Okuda K 1995 *Physica* C **253** 135
[2] Kojima K M, Fudamoto Y, Larkin M, Luke G M, Merrin J, Nachumi B, Uemura Y J, Motoyama N, Eisaki H, Uchida S, Yamada K, Endoh Y, Hosoya S, Sternlieb B J and Shirane G 1997 *Phys. Rev. Lett.* **78** 1787
[3] Ami T, Crawford M K, Harlow R L, Wang Z R, Johnston D C, Huang Q and Erwin R W 1995 *Phys. Rev.* B **51** 5994
[4] Motoyama N, Eisaki H and Uchida S 1996 *Phys. Rev. Lett.* **76** 3212
[5] Rosner H, Eschrig H, Hayn R, Drechsler S-L and Malek J 1997 *Phys. Rev.* B **56** 3402
[6] Dou S X, Guo S J, Liu H K and Easterling K E 1989 *Supercond. Sci. Technol.* **2** 308
[7] Wada J, Wakimoto S, Hosoya S, Yamada K and Endoh Y 1995 *Physica* C **244** 193
[8] Zhang G M, Mai W J, Li F Y, Bao Z X, Yu R C, Lu T Q, Liu J and Jin C Q 2003 *Phys. Rev.* B **67** 212102
[9] Yoshida M, Tajima S, Koshizuka N, Tanaka S, Uchida S and Ishibashi S 1991 *Phys. Rev.* B **44** 11997
[10] Lines D R, Weller M T, Currie D B and Ogborne D M 1991 *Mater. Res. Bull.* **26** 323
[11] Maiti K, Sarma D D, Mizokawa T and Fujimori A 1998 *Phys. Rev.* B **57** 1572
[12] Altermatt D and Brown I D 1985 *Acta Crystallogr.* B **41** 244
[13] Zuo J M, Kim M, O'Keeffe M and Spence J C H 1999 *Nature* **401** 49
[14] de Graaf C and Illas F 1999 *Phys. Rev.* B **63** 014404
[15] Hoang N N, Huynh D C and Phan M H 2006 *Solid State Commun.* **139** 456
Thanh P Q, Nhat H N and Chinh H D 2006 *J. Magn. Magn. Mater.* doi:10.1016/j.jmmm.2006.11.031
[16] Valach F, Hoang N N, Maris T, Saunders A, Cowley A, Watkin D J and Prout C K 2003 *Progress in Coordination and Bioinorganic Chem* ed M Melník and A Sirota (Bratislava: STU Press)
Valach F 1999 *Polyhedron* **18** 699
[17] Maiti K and Sarma D D 2002 *Phys. Rev.* B **65** 174517
[18] Shin Y J, Manova E D, Dance J M, Dordor P, Grenier J C, Marquesteut E, Doumere J P, Pouchard M and Hagenmuller P 1992 *Z. Anorg. Allg. Chem.* **616** 201
[19] Hoang N N and Huynh D C 2007 Structure, Raman and transport properties of the uranium-doped Ca_2CuO_3, at press
Phung Q T, Hoang N N and Huynh D C 2007 Possible phonon-assisted electron hopping conduction in the uranium doped Ca_2CuO_3 *J. Korean Phys. Soc.* at press
[20] JCPDS Files No. 34-0282 (Ca_2CuO_3); no37-1497 (CaO); no5-661 (CuO).
[21] Jouanneaux A 1999 *CPD Newslett.* **21** 13
[22] Krumm S 1994 *Acta Universitatis Carolinae Geol.* **38** 253
[23] Burnett M N and Johnson C K 1996 *ORTEP/1/Report* ORNL-6895 Oak Ridge National Laboratory, TN, USA